Macromolecules

ARTICLE

pubs.acs.org/Macromolecules

Janus Triad: Three Types of Nonspherical, Nanoscale Janus Particles from One Single Triblock Terpolymer

Andrea Wolf,[†] Andreas Walther,[*,‡] and Axel H. E. Müller[*,†]

[†]Macromolecular Chemistry II, University of Bayreuth, D- 95447 Bayreuth, Germany

[‡]DWI at the RWTH Aachen, D-52056 Aachen, Germany

Supporting Information

ABSTRACT: We report the synthesis of three different Janus topologies from one single specific triblock terpolymer, poly(*tert*-butoxystyrene)-*block*-polybutadiene-*block*-poly(*tert*-butyl methacrylate) (tSBT). By controlling the phase transitions via pretreatment and cross-linking conditions of the lamella−cylinder equilibrium bulk morphology of the polymer, we were able to obtain Janus cylinders, sheets, and previously unknown Janus ribbons. Here, a delicate balance of experimental parameters allows to manipulate the microphase morphologies as needed. The attained control even realizes the trapping of a complex intermediate phase, where every second intercylinder distance in the lamella−cylinder morphology is connected by a thin lamella. Furthermore, we also show that casting from a selective solvent can be used to access the lamella−sphere morphology and fabricate spherical Janus particles. What is more, poly(*tert*-butoxystyrene) can be hydrolyzed to polyhydroxystyrene, which is water-soluble at high pH and thus pH-responsive. It also represents a reaction site for further functionalizations and is thus an attractive alternative to the commonly used polystyrene. We furthermore present cryo-TEM images of water-soluble Janus cylinders that include one of the best quasi in-situ real-space proofs for the Janus character of nanosized, anisometric polymer-based particles.

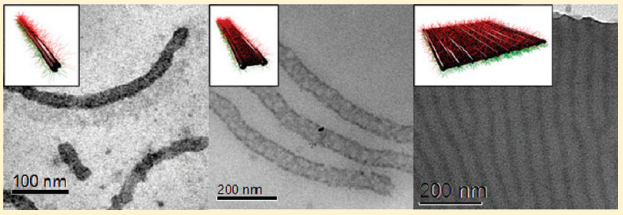

INTRODUCTION

Janus particles (JPs) are bicompartmentalized, noncentrosymmetric colloids. Their two sides or surfaces are different in terms of their chemical and/or physical properties. JPs have gained much interest during the past years. Several reviews concerning their synthesis[1] and supramolecular organization[2,3] and with a special focus on polymeric JPs[2,4] appeared in recent years. Their noncentrosymmetric architecture provides JPs with unique properties not accessible for homogeneous analogues. For instance, the broken symmetry leads to the formation of a variety of complex superstructures,[3,5−7] which cannot be obtained from simple particles, thus representing fascinating building blocks for the constructions of hierarchical assemblies and materials. Furthermore, they have a high tendency to adsorb and assemble at interfaces due to their bicompartment character, thereby lowering interfacial tension significantly further as compared to homogeneous particles or block copolymers.[8−10]

A broadly applied method for the synthesis of spherical JPs is the desymmetrization of spherical homogeneous particles in the micrometer range.[7,11,12] On the contrary, the synthesis of nonspherical JPs as well as the production of particles in the nanometer range has remained challenging, where bottom-up self-assembly approaches present the most elegant methodology to solve this problem. One method that can accomplish both these tasks is based on converting triblock terpolymer bulk structures via selective cross-linking of the middle block.[13,14] Apart from spherical particles,[15] also cylinders[5,16] and sheets or discs[3,17] can be produced on a multigram scale with this method. So far, polystyrene-*block*-polybutadiene-*block*-poly(methyl methacrylate) (SBM) and polystyrene-*block*-polybutadiene-*block*-poly(*tert*-butyl methacrylate) (SBT) triblock terpolymers were used as polymeric materials. Additionally, each type of Janus particle architecture has so far relied on tailoring the interactions and the weight fraction of the middle block to target specific equilibrium phase morphologies suitable for the fabrication of the aimed dimensionality. Moreover, polystyrene is considered as a "dead" and nonfunctional material, which at best imparts an amphiphilic character into suitably modified Janus particles via its hydrophobicity. The harsh chemistries required for a near-quantitative functionalization (e.g., sulfonation) of PS in confined particle geometries and in presence of partly labile cross-links within the PB core (e.g., disulfide bonds) are hardly applicable. Therefore, a replacement into an already functional polymer side would be highly beneficial to be able to control the physics and chemistry of both sides. This calls for a new synthetic concept and for the development of an understanding of how to manipulate the microphase morphologies to alter the dimensions of the resulting particles.

Therefore, we turned to poly(*tert*-butoxystyrene) (PtBS) as first block in the synthesis of the relevant triblock terpolymer.

Received: September 7, 2011
Revised: October 13, 2011
Published: November 03, 2011

ACS Publications © 2011 American Chemical Society

The predominantly chosen method for the synthesis of PtBS is living anionic polymerization.[18−20] PtBS can be hydrolyzed to polyhydroxystyrene (PHS), a pH-sensitive weak polyelectrolyte. In contrast to PS, PHS is soluble in water at high pH and as such represents a stimuli-responsive segment.[21,22] As a main benefit, the hydroxyl group also allows simple chemical modifications in different directions, which further increases the versatility of this polymer. Some isolated reports exist on the utilization of PHS in the field of block copolymers and for stimuli-responsive micelles because of these interesting properties.[21−28]

Herein we present the synthesis of polymeric Janus particles from a triblock terpolymer (poly(*tert*-butoxystyrene)-*block*-polybutadiene-*block*-poly(*tert*-butyl methacrylate) (tSBT)) containing a poly(*tert*-butoxystyrene) segment as one of the sides.

We will show how careful adjustment of the microphase-segregated structures and the cross-linking conditions can be used to create four different types of Janus nanoparticles from one single triblock terpolymer, where we will however focus on the rare nonspherical particles. Furthermore, we demonstrate the water solubility and anisotropic character of our JPs after hydrolysis of PtBS and PtBMA to PHS and PMAA, respectively.

EXPERIMENTAL SECTION

Materials. *p*-(*tert*-Butoxy)styrene and *tert*-butyl methacrylate (both Aldrich) were degassed, treated with dibutylmagnesium (*tert*-butoxystyrene) or trialkylaluminum (*tert*-butyl methacrylate), and distilled or condensed, respectively.[5] *sec*-Butyllithium (1.4 M in cyclohexane, Aldrich), acetonitrile (anhydrous 99.8%, Aldrich), chloroform (p.a. grade, Fisher Scientific), dioxane (p.a. grade, Fisher Scientific and Riedel de Haën), *tert*-butanol (p.a. grade, Merck), THF (technical grade for Soxhlet extraction, p.a. grade, VWR), sulfur monochloride (98%, Aldrich), photoinitiator 2,4,6-trimethylbenzoyldiphenylphosphine oxide (Lucirin TPO (BASF)), and trimethylsilyl iodide (purum ≥98%, Fluka) were used as received. Water was purified with a Milli-Q water purification system by Millipore.

Instrumentation. *Gel permeation chromatography−multiangle light scattering* (GPC-MALS) measurements were performed at room temperature using a GPC system with three 30 cm PSS SDV columns (10^4, 10^5, 10^6 Å), equipped with a Wyatt DAWN HELEOS light scattering detector (50 mW solid state laser; λ = 658 nm) and an Agilent HPLC-assembly. THF was used as eluent (flow rate 0.8 mL/min). Data evaluation was carried out with the Astra Software.

Small-angle X-ray scattering (SAXS) measurements of a solvent-cast free-standing polymer film of ca. 200 μm thickness were performed with a rotating anode Bruker Microstar microfocus X-ray source (Cu Kα radiation, λ) 1.54 Å) with Montel Optics with a measurement time of 4 h. The beam was further collimated with four sets of slits, resulting in a beam area of about 1 × 1 mm at the sample position. Scattering intensities were measured using a Bruker AXS 2D area detector. The sample-to-detector distance was 1.5 m. The magnitude of the scattering vector is given by $q = (4\pi/\lambda) \sin \theta$, where 2θ is the scattering angle.

Photo-cross-linking was induced with a HOENLE UVA HAND 250 lamp (cutoff <350 nm), equipped with water cooling for the sample holder.

Sonication treatment was performed with a Branson model-250 digital sonifier with a 1/8 in. diameter tapered microtip (200 W at 100% amplitude).

Scanning force microscopy (SFM) images were taken on a Veeco Digital Instruments Inc. Dimension 3100 closed loop microscope in tapping mode. Offline data processing was done using the Nanoscope Software V6.14R1.

Transmission electron microscopy (TEM) images were recorded in bright field mode with a Zeiss CEM 902 transmission electron microscope operated at 80 kV and a LEO 922 OMEGA transmission electron microscope operated at 200 kV. Polymer films were cut into thin sections at room temperature using a Reichert-Jung Ultracut E microtome equipped with a diamond knife. Data evaluation and processing was carried out with Soft Imaging Viewer, Digital Micrograph 365 Demo software and Image Tool.

Synthesis of Poly(*tert*-butoxystyrene)-*block*-polybutadiene-*block*-poly(*tert*-butyl methacrylate). tSBT was synthesized via living anionic polymerization. Having become a standard method by now, the general procedure of this polymerization technique is described in detail elsewhere.[5] In short, the calculated amount of *sec*-butyllithium initiator (0.22 mL, 0.31 mmol) was added to the *p*-*tert*-butoxystyrene solution in THF at −78 °C, and after 1 h butadiene was added to the mixture at −78 °C and polymerized at −30 °C for 5 h. Thereafter, the reaction mixture was treated with a 5-fold excess of 1,1-diphenylethylene relative to the amount of initiator before the addition of tBMA at −60 °C and subsequent polymerization at −40 °C for 2 h.

Film Casting. The respective amount of tSBT with Lucirin TPO was dissolved in the desired solvent in a crystallization dish or small glass vial. After that, evaporation of the solvent took place for 2 weeks (crystallization dish) or several days (vial) at room temperature, and the films were dried in vacuum for 24 h at room temperature.

Photo-Cross-Linking with Lucirin TPO. Polymer films, co-cast with 30 wt % of Lucirin TPO, were exposed to the radiation of a UV lamp for 3.5 h. Subsequently, the films were Soxhlet extracted for several days with THF.

Cross-Linking with Sulfur Monochloride (S_2Cl_2). A piece of polymer film was swollen in acetonitrile for 1 day. 5−10 vol % of S_2Cl_2 was added via a syringe, and the cross-linking took place at room temperature overnight. In the case of Janus ribbons, films were swollen in an acetonitrile/decane emulsion that needed constant, not too strong stirring (ca. 130 rpm) to avoid large-scale demixing of the two solvents. Cross-linking time was 7 h. After the reaction, the films were washed three times with aprotic solvents acetonitrile and dioxane and purified via Soxhlet extraction with THF for 1−3 days. In the case of Janus spheres, a vial containing a piece of cast film was placed in a desiccator together with a vial containing few drops of S_2Cl_2. After applying vacuum, cross-linking took place under passive vacuum for 3 days.

Sonication. Cross-linked material was dispersed in dioxane to give dispersions of an approximate concentration of 1 mg/mL. Portions of about 20 mL were then treated with an ultrasound sonication tip under water cooling. The typical settings were a pulse of 2 s, 5−10 s of pause, sonication time of 30−90 s, and amplitude of 30%. Afterward, the solutions were filtrated using a 5 μm PTFE filter and freeze-dried.

Hydrolysis of Janus Cylinders. Janus cylinders were dissolved in $CHCl_3$ to give a solution of ca. 1.5 wt %. After degassing for ∼20 min, a 1.3-fold excess of trimethylsilyl iodide (TMSI) regarding the amount of addressed *tert*-butoxy groups was introduced to the solution with a syringe under nitrogen. Afterward, the mixture was stirred for 3 h at 60 °C and then treated with few mL of basic Milli-Q water (pH 12−14, addition of NaOH). Subsequent dialysis against dioxane, water/dioxane (1/1), and water of different pH values was used for the work-up. A regenerated cellulose Spectra/Por dialysis membrane with molecular weight cutoff of 50 000 was used.

Preparation of TEM Samples. Microtome-cut ultrathin film sections were exposed to OsO_4 vapor for 60 s for preferential staining of the polybutadiene block (appears black). Liquid TEM samples were solvent evaporated from solutions with a concentration of 1 mg/mL on carbon-coated copper grids. For aqueous solutions, grids were rendered hydrophilic via a plasma treatment and the sample was blotted after 30 s. For cryogenic transmission electron microscopy (cryo-TEM) studies, a drop of the sample, dissolved in water or toluene, was put on a lacey

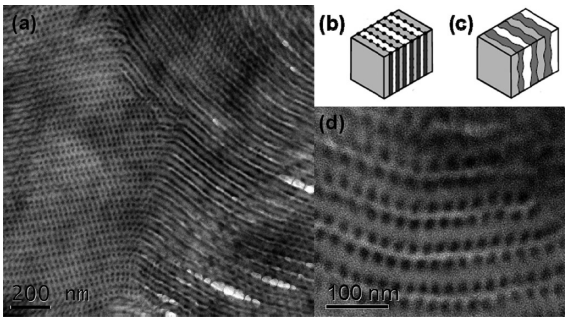

Figure 1. TEM micrographs (a, d) of ultrathin sections of a tSBT film stained with OsO_4 (PB appears black, PtBS gray and PtBMA white) and two cartoons displaying a lamella-cylinder (b) and an undulated lamellar morphology (c).

carbon-coated copper grid, where most of the liquid was removed with blotting paper, leaving a thin film stretched over the lace. The specimens were instantly vitrifed by rapid immersion into liquid ethane (aqueous samples) or nitrogen (toluene) and cooled to ~90 K by liquid nitrogen in a temperature-controlled freezing unit (Zeiss Cryobox, Zeiss NTS GmbH, Oberkochen, Germany). The temperature was monitored and kept constant in the chamber during all of the sample preparation steps. After freezing the specimen it was inserted into a cryo-transfer holder (CT3500, Gatan, München, Germany) and transferred to the Zeiss LEO 922 OMEGA TEM. Examinations were carried out at temperatures around 90 K.

■ RESULTS AND DISCUSSION

Bulk Morphology of tSBT. All Janus particles in this work were synthesized from one single poly(*tert*-butoxystyrene)-*block*-polybutadiene-*block*-poly(*tert*-butyl methacrylate) triblock terpolymer (abbreviated as tSBT in the following). It was synthesized via living anionic polymerization in the same manner as previously described for polystyrene-*block*-polybutadiene-*block*-poly(methyl methacrylate).[29] Gel permeation chromatography combined with multiangle light scattering (GPC-MALS) showed a molecular weight of 163 000 g/mol and a polydispersity index of 1.01 (Supporting Information, Figure S1). The weight fractions of the three blocks were calculated from NMR to be $tS_{46}B_{16}T_{38}$. After film-casting from chloroform, we examined the resulting bulk structure of tSBT by transmission electron microscopy (TEM) and small-angle X-ray scattering (SAXS). The bulk structure of this block terpolymer corresponds to a lamella−cylinder (lc) morphology. Figure 1 shows a TEM micrograph of an OsO_4-stained ultrathin section of tSBT. The polybutadiene (PB) cylinders (appearing black) are surrounded by alternating lamellae of poly(*tert*-butoxystyrene) (PtBS) (gray) and poly(*tert*-butyl methacrylate) (PtBMA) (white). The PtBMA phase appears white due to electron-beam-induced degradation. The diameter of the polybutadiene cylinders is 14 ± 1.8 nm, and the distance between the centers of two cylinders is in the range of 22 nm while the long period of the lamellar structure is 68 nm. Note that the TEM micrograph may not reflect the absolute dimensions as staining and electron-induced degradation of the PtBMA may alter the exact distances to some extent. With respect to the following results, it is important to note that a morphology with undulated lamellae, as shown in Figure 1c, could not be observed. The magnified image (see Figure 1d) does not indicate any thin lamellar connections between the PB cylinders.

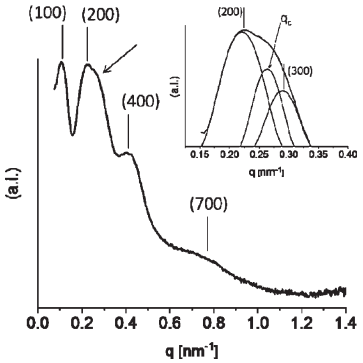

Figure 2. SAXS curve of tSBT with a characteristic shoulder indicated by the arrow. Inset shows the deconvolution of the shoulder revealing the underlying correlation distance of the cylinders.

The result of the SAXS measurements is in agreement with the observed lamella−cylinder morphology. Figure 2 depicts the scattering curve of tSBT exhibiting the typical integer reflexes of a lamellar morphology. Additionally, the 200 peak is rather broad and exhibits a shoulder. Its deconvolution results in three peaks that can be assigned to the 200 and 300 reflexes and the primary reflex of the correlation distance between the cylinders. This characteristic spacing can be calculated to 21.8 nm. The calculated long period is 60 nm. In comparison, the values measured in TEM micrographs are 22 nm for the cylinder distance and 68 nm for the long period and therefore in good agreement.

Preparation of Janus Particles. Two different approaches were used to cross-link the PB domains and prepare Janus particles. Photo-cross-linking was performed using 2,4,6-trimethylbenzoyldiphenylphosphine oxide (Lucirin TPO) as radical initiator, which was cocast with the polymer. The incorporation of Lucirin TPO does not alter the morphology of tSBT-films as concluded from TEM images of the bulk structures (Supporting Information, Figure S2). The other method employed sulfur monochloride, S_2Cl_2, as cross-linking agent. Here, the polymer film was swollen in acetonitrile before the introduction of the cross-linking agent.

Photo-cross-linking resulted in well-defined Janus cylinders after dispersing the polymer film in dioxane, a good solvent for all three blocks of the terpolymer (Figure 3a). To decrease the length and thus to enhance the solubility of the resulting particles, the cylinders were sonicated (Figure 3b). These and all following TEM images are nonstained if not stated otherwise.

The evaluation of the core diameter of the core−corona structures visible in the TEM images yields values in the range of 22 nm. This value exceeds the measured diameter of the PB cylinders of 14 ± 1.8 nm in the bulk structure. Furthermore, the heights of the structures by scanning force microscopy (SFM) are in the range of 15 nm (Figure 3d). Considering the presence of additional corona on top and below of the PB cylinder (Figure 3a), a slightly flattened appearance of the PB cylinder is indicated when adsorbed onto surfaces.

In contrast to photo-cross-linking, the procedure of using S_2Cl_2 as cross-linker involves a previous swelling of the polymer film in acetonitrile. After addition of S_2Cl_2, during the so-called cold vulcanization process, disulfide bonds between the polybutadiene double bonds form. Similar to the case of photo-cross-linking, we expected the formation of Janus cylinders because of the lc morphology. Surprisingly, however, after cross-linking through cold vulcanization followed by sonication, two-dimensional

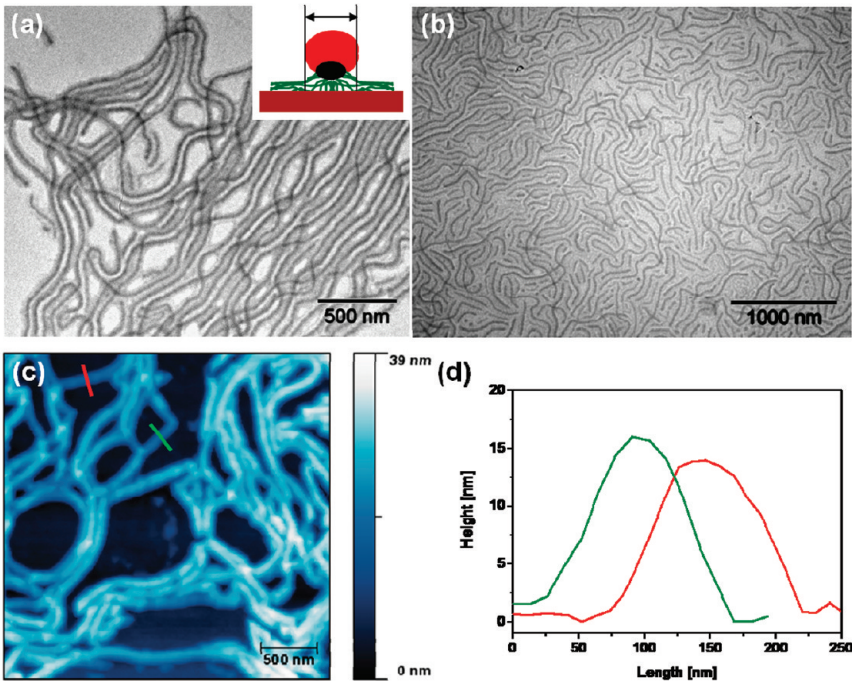

Figure 3. TEM micrographs of Janus cylinders before (a) and after (b) sonication and SFM height image of Janus cylinders (c) with corresponding cross sections (d).

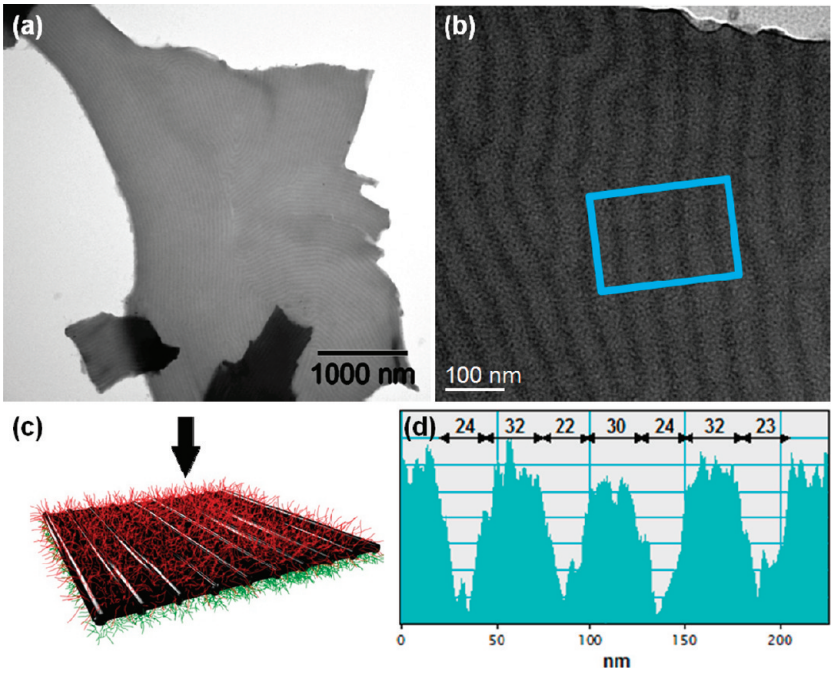

Figure 4. TEM images of Janus sheets obtained from tSBT after 1 (a) and 5 (b) days of swelling in acetonitrile, cross-linked with S_2Cl_2, with (d) analysis of the cross section indicated in micrograph (b). The schematic drawing (c) indicates the line of sight onto the Janus sheets.

Janus sheets instead of cylinders were obtained. Interestingly, the TEM micrographs show that the PB lamella is not of uniform thickness. Instead, clear, well-spaced undulations can be observed (Figure 4b). PB cylinders (darkest areas) can be observed that are connected by a PB layer, clearly thinner than the cylinders themselves (consequently brighter in the TEM image). Therefore, a phase transition in the morphology has occurred. Note that this transition is solely caused by the reaction with S_2Cl_2 and not already upon addition of the swelling solvent as confirmed by a detailed TEM study (Supporting Information, Figure S3). The concurrent volume increase of the PB phase during incorporation of the

dx.doi.org/10.1021/ma2020408 |*Macromolecules* 2011, 44, 9221–9229

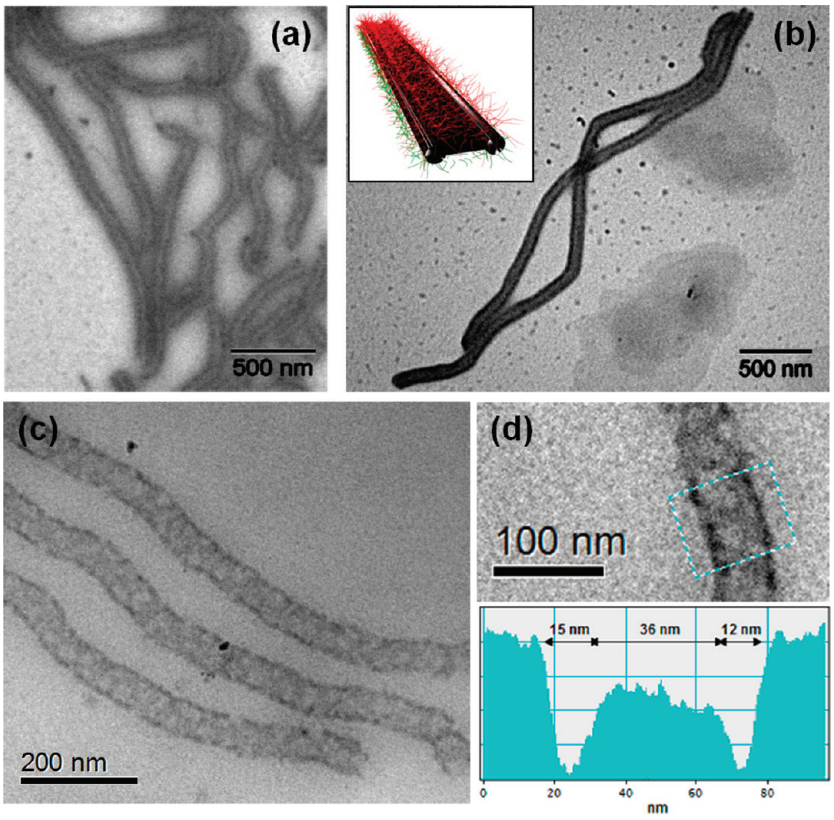

Figure 5. TEM images of dried Janus ribbons (a, b) including a scheme of one Janus ribbon (inset in b) and cryo-TEM images in vitrified toluene (c, d) with analysis of the cross section indicated in micrograph (d).

bulky S_2Cl_2 and altered interfacial tensions among the various blocks trigger this phase transition.

The structure developing during the process is best described as an undulated-lamellar (ul) morphology. A section analysis further visualizes this structure (Figure 4d). The cross section is based on the gray scale originating from the contrast variations within the sample. The thicker and darker cylinders can clearly be distinguished from the thinner and brighter connecting PB parts. The gray scale analysis shows a diameter of the cylinders of ca. 23 nm and a width of the connecting PB parts in the range of 30−32 nm, thus exhibiting slightly larger dimensions than the cylinder packing in the bulk structure. The swelling and the addition of S_2Cl_2 cause an increase of the volume of the PB domains, which is reflected in the final dimensions of the Janus sheet structure. As the thinner parts of the PB layer are prone to fracture, most of the sheets have very clear particle edges along the cylinder lines and favor rectangular materials upon prolonged sonication.

With the aim of achieving a continuous PB lamella to increase the stability of the Janus sheets, we added other solvents (e.g., decane) that have a better ability to swell the PB phase than acetonitrile. However, tSBT is soluble in decane and to prevent the complete dissolution of tSBT while still keeping decane as a good swelling agent for PB, a mixture of decane and acetonitrile was used in a ratio of 1:1. The two solvents are not fully miscible but form an emulsion upon stirring. After 14 h of swelling in the steadily stirred decane/acetonitrile emulsion, tSBT was cross-linked with S_2Cl_2 for 7 h. Surprisingly, instead of continuous Janus sheets, a totally new type of Janus particle was obtained, i.e., Janus ribbons (Figure 5). Therein, exactly two Janus cylinders are connected along their major axis via a thin PB layer, forming a ribbon-type structure. The population is fascinatingly homogeneous with respect to the exclusive connection of only two cylinders. Individual Janus cylinders are nearly absent, and trimeric cylinders do not exist. Additionally, the ends of both connected cylinders terminate at similar distance, indicating that the bands extend throughout the complete domain of the microsphase-segregated morphology and that sonication chops fully extended Janus ribbons into shorter pieces.

Unlike in the case of Janus sheets, where a complete phase transition from an lc to an ul morphology takes place, a different phase transition occurs during the formation of the Janus ribbons. A connecting PB layer is formed only in every second interspace of the original PB cylinders. Therefore, we suggest that the precise PB layer formation might be influenced by a wave-function-like instability occurring during the structure formation in the stirred emulsion. Such hydrodynamic instabilities might be assisted by the shear forces caused by the steady stirring of the emulsion. For cylindrical particles like polymer threads sinusoidal distortions, which lead to a breakup of the particles into spheres, are also known to be caused by Rayleigh−Plateau instabilities.[30]

Further investigation of the synthesis pathway showed that a sufficient swelling time is necessary for a complete phase transition. After only 7 h of swelling and subsequent cross-linking TEM micrographs indicate the development of only few Janus ribbons whereas mainly Janus cylinders are present (Supporting Information, Figure S4).

This observation together with the TEM images of tSBT (Figure 1) which show an lc morphology supports the

above-described pathway and opposes the possibility that the Janus ribbons originate from an initially formed undulated lamellar morphology which is then broken in every second interspace. Additionally, the formation of ribbons in decane/acetonitrile emulsion, in contrast to sheet formation in pure acetonitrile (stirred and unstirred), illustrates the strong influence of the swelling agent and the hydrodynamic forces.

Strikingly, despite the challenging conditions, the Janus ribbon synthesis proved to be highly reproducible, thus corresponding to a remarkably defined and robust pathway for the phase transition. This points to the fundamentally important discovery of a defined intermediate phase during the phase transition from a lamella-cylinder to an undulated-lamella morphology.

To gain further insight into the structure of the Janus ribbons and their behavior in solution, they were also investigated by cryogenic transmission electron microscopy (cryo-TEM) in toluene solution. Figure 5c,d shows micrographs taken of a sample of Janus ribbons in toluene and a cross-section analysis for one ribbon. The gray scale analysis visualizes the structure of the PB layer of the Janus ribbons with two limiting cylinders at the boundaries (darker in the image, lower gray value) connected by a thinner layer of PB (lighter in the image). It indicates a diameter of 12−15 nm for the cylinders and 36 nm for the interspace. Because of swelling and lower contrast in cryo-TEM, the dimensions of the cylindrical parts at the lateral boundaries of the ribbon can be underestimated. In comparison, lateral cylinders of the ribbons in TEM of a dried sample (Figure 5a,b) are 24 ± 7 nm and their interspaces 37 ± 9 nm. These ribbon dimensions are similar to the dimensions of the Janus sheets in TEM of a dried sample (cylinders ≈23 nm, interspaces ≈31 nm). These were also swollen and treated with S_2Cl_2, thus illustrating that both structures, ribbons and sheets, originate from the same lc morphology. Consequently, the higher radius of the cylinders in the final ribbons compared to the bulk phase and the radically cross-linked Janus cylinders is due to the incorporated S_2Cl_2 similar to the case of Janus sheets.

The susceptibility of the lamella−cylinder equilibrium bulk morphology to phase transitions also prompted us to explore whether suitable solvent casting could be used to obtain the lamella−sphere (ls) morphology suitable for the fabrication of Janus spheres. Indeed, it turned out that *tert*-butanol, a good solvent for both end blocks, PtBS and PtBMA, leads to the development of spherical PB domains at the interface of an overall lamellar structure. Obviously, the strong ability to swell the end blocks of the tSBT triblock terpolymer, while being a nonsolvent for the middle block, leads to the development of the ls bulk structure, which is a defined nonequilibrium state that cannot relax into the lc phase due to the slow dynamics in the bulk state. Subsequent cross-linking of the thereby obtained films with S_2Cl_2 in the gaseous phase can be used to lock the morphology and produce Janus spheres. Since the focus of this article is however set on nonspherical Janus particles, we only show the corresponding TEM images in the Supporting Information (Figure S5).

Summarizing the first part, we were able to synthesize nanosized JPs with three different nonspherical topologies from one single tSBT triblock terpolymer, which are Janus cylinders, Janus ribbons, and structured Janus discs, in addition to spherical Janus beads. This represents a significant simplification of the production of different Janus architectures. We accomplished that by the careful adjustment of pretreatment and cross-linking conditions of its bulk morphology. Photo-cross-linking without prior swelling led to Janus cylinders. This was expected because tSBT showed an lc

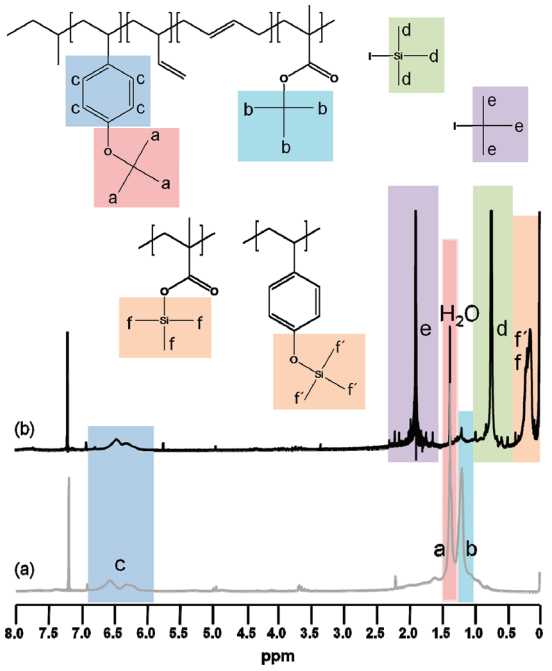

Figure 6. ^{1}H NMR spectra illustrating the hydrolysis of Janus cylinders recorded in $CDCl_3$: (a) before hydrolysis and (b) after addition of TMSI and 3 h at 60 °C.

morphology after film-casting from chloroform. However, if the polymer film was swollen in acetonitrile prior to cross-linking with S_2Cl_2, the morphology changed to an undulated lamella one in which the original cylinders still exist in the form of thicker parts in the newly formed PB lamella. After cross-linking and sonication, this morphology results in sheet-like JPs. Most surprising is the discovery of the novel topology of Janus ribbons (with a flattened dimension compared to cylinders). They formed when the original polymer film was swollen in a stirred acetonitrile/decane emulsion. Exclusively two cylinders became connected by a newly developed PB layer. This ribbon-like structure was then preserved by cold vulcanization.

Hydrolysis of the Janus Cylinders. Apart from the versatility of the tSBT triblock terpolymer concerning the synthesis of different Janus structures, it also features the interesting PtBS block, which was chosen for the possibility of hydrolysis into pH-responsive polyhydroxystyrene (PHS). The pK_a of linear PHS is reported at ∼10,[22,31] and Janus particles with a pH-dependent water-soluble PHS side can be created. Furthermore, the hydrolysis of PtBMA results in poly(methacrylic acid) (PMAA) hemicylinders, which are well water-soluble at pH ≥ 4. Consequently, HSBT Janus particles made from tSBT are potentially water-soluble and pH-responsive which extends the range of self-assembly and enables applications in aqueous media. Additionally, the hydroxyl group allows further functionalization of the Janus particles. In the following we focus on the solution properties of the Janus cylinders.

For the hydrolysis we chose the reaction with trimethylsilyl iodide (TMSI). This mild method can be used for esters and ethers and works already at room temperature or at slightly elevated temperatures.[32,33] First, the *tert*-butoxy group is converted to a silyl ester (PtBMA) or ether (PtBS), respectively, by TMSI, and then the actual hydrolysis follows through addition of water or methanol.

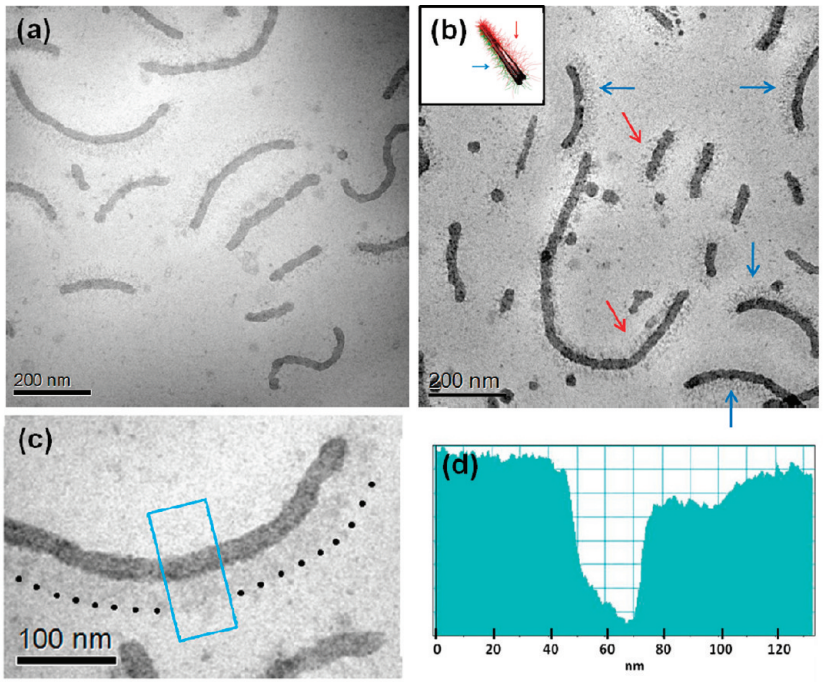

Figure 7. Cryo-TEM images of hydrolyzed Janus cylinders at pH ≈ 10 (a, b, c) with gray scale analysis (d) of the cross section indicated by blue line in the micrograph (c). Dotted line in micrograph (c) visualizes the boundary of the PMAA corona.

Figure 6 presents the ^{1}H NMR spectra of Janus cylinders before and after reaction with TMSI at 60 °C, yet before the final hydrolysis took place.

The spectra clearly show the substitution of the *tert*-butoxy group to a near-quantitative degree, which then hydrolyze fully upon addition of aqueous methanol. Both peaks corresponding to the *tert*-butyl groups are strongly diminished, and only signals of the polymer backbone remain. A comparison of the silyl ester/ether signal f/f′ with the signals of the aromatic units results in a conversion of above 90%. The very sharp peak at 1.36 ppm in the spectra (b) originates from residual water.

Solution Structure of Water-Soluble Janus Cylinders. To investigate the solution structure of these hydrolyzed Janus cylinders, cryo-TEM images in water (pH ≈ 10 and pH ≈ 13) in the presence of 100 mM CsCl were recorded. Cryo-TEM has the distinct advantage that the extent of staining with heavy ions depends on the degree of ionization of the polyelectrolyte brushes, their brush density, and thus the overall tendency to confine counterions within the brush. This is the reason why poly(ethylene oxide) or other nonionic water-soluble polymer coronas (of micelles or particles) can often not be visualized due to the unfavorable staining behavior and contrast, whereas strong polyelectrolyte brushes are rather easy to resolve using appropriate ionic additives. We herein applied this principle with the aim to visualize the biphasic character of fully water-soluble Janus cylinders at appropriate pH values, where both corona sides are differently stained simply for their different degrees of ionization.

Figure 7 displays images of the Janus cylinders at pH 10, where the PHS block only carries a minor fraction of charges, in particular compared to the basically quantitatively deprotonated PMAA side. Various unimolecularly dispersed cylinders can be observed in which a corona is solely visibly on one side. Figure 7c,d displays a further closeup on one cylinder and the complementing cross-sectional gray scale analysis. The Janus character of the cylinders is remarkably well visible. At the lower side of the well-visible dark cylinder in Figure 7c, a corona part with condensed Cs^+ counterions is evident, whereas no corona can be observed at the upper side. Given the large difference of the pK_a values of PMAA and PHS, we can reasonably suggest that the visible corona consists of the completely deprotonated PMAA. Because of its high charge density at pH 10, a large amount of Cs^+ counterions is condensed inside its corona. In contrast, PHS with its pK_a around 10 is far less ionized, especially as it was shown that the pK_a can increase for brush-like structures as compared to linear analogous. This behavior was found earlier by us for multiarm star-shaped polyanions.[34] Thus, at pH 10, the fraction of deprotonated PHS units is small, and consequently very little Cs^+ ions can accumulate within the PHS corona. Therefore, it is not visible adjacent to the dark PB core and PMAA corona. It is also important to note that the calculated diameter of the dark cylinder only amounts to 23 ± 3 nm. This corresponds to the PB cylinder alone and further indicates that the PHS part is dissolved and not part of the dark cylindrical core.

The exclusive visibility of the PMAA corona at one side of the cylinder represents one of the most convincing real-space proofs of the biphasic character of water-soluble polymeric Janus nanoparticles. It furthermore establishes that the phase segregation is fully retained during the transfer of the cross-linked bulk structure into solution and does not vanish due to a potential entropically favored chain mixing of the two sets of brush arms on the cross-linked PB cylinder. The PMAA corona can be found at the cylinders in all four directions with respect to the image (Figure 7b, blue arrows). This confirms the absence of any artifacts of the imaging process. Cylinders that seem to have a corona on both sides are simply imaged from

dx.doi.org/10.1021/ma2020408 |*Macromolecules* 2011, 44, 9221–9229

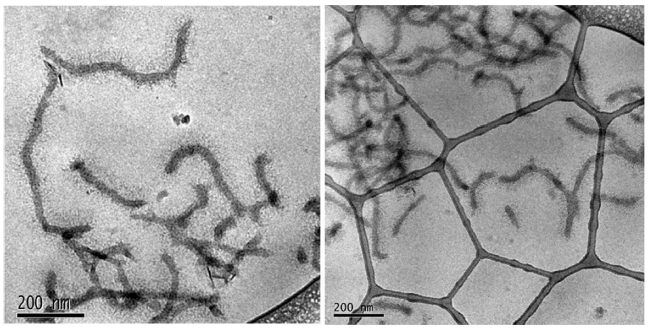

Figure 8. Cryo-TEM images of hydrolyzed Janus cylinders at pH 13.

the top (red arrows) because of the rotational freedom of the cylinders within the thin water film.

The situation looks different when studying cryo-TEM images of hydrolyzed Janus cylinders at pH 13 (recorded in the presence of 100 mM CsCl). Figure 8 shows two typical images. As anticipated, in contrast to the cylinders shown above, every cylinder displays a corona on both sides, fully surrounding the central PB cylinder. This is due to the fact that now not only PMAA but also PHS is deprotonated to a high degree and therefore binds large amounts of Cs^+ ions. The average diameter of the cylindrical cores is 22 ± 2 nm and therefore the same as for pH 10. This underlines the fact that the PHS corona is soluble for both pH values; it just remains invisible at pH 10 because of insufficient counterion capture at lower ionization.

CONCLUSIONS

We have demonstrated how the careful choice of solvent and cross-linking conditions can be used to manipulate triblock terpolymer bulk structures in a way that allows synthesizing three different types of nonspherical Janus particles as well as spherical ones from one single triblock terpolymer. We were able to obtain Janus sheets, Janus cylinders, and an intermediate new structure, Janus ribbons. The successful preparation of all these structures relies on a thorough understanding of how to manipulate the bulk morphologies into equilibrium and nonequilibrium structures. The intermediate fraction of PB of 16 wt % facilitates transformations into spherical and lamellar domains that would usually be only stable at much smaller or larger weight fractions (at moderate interfacial tension/incompatibility between A and C), respectively. Selective solvent casting proved useful to access the nonequilibrium ls morphology and generate Janus spheres. On the other hand, the surprising observation of Janus ribbons points to the fundamentally important discovery of a defined intermediate phase during the phase transition from the lamella-cylinder to the undulated-lamella morphology. Overall, this beneficial and simple way to tune bulk morphologies drastically simplifies the access routes toward asymmetric soft Janus particles with nanometer dimensions on the multigram scale. We expect that the considerations herein can be applied to other terpolymer systems and allow to generate Janus particles of higher functionality from a single triblock terpolymer with moderated efforts. We also introduced the use of poly(*tert*-butoxystyrene) instead of polystyrene in the synthesis, which can be hydrolyzed to polyhydroxystyrene, featuring stimuli responsiveness and water solubility and opening possibilities for the modification of the PHS hydroxyl group toward tailored functionalities in the future. The water solubility and stimuli responsiveness expand possible fields of application for such Janus particles to aqueous media.

ASSOCIATED CONTENT

Supporting Information. GPC-MALS curve of tSBT and additional TEM micrographs. This material is available free of charge via the Internet at http://pubs.acs.org.

AUTHOR INFORMATION

Corresponding Author

*E-mail: walther@dwi.rwth-aachen.de (A.W.); axel.mueller@uni-bayreuth.de (A.H.E.M.).

ACKNOWLEDGMENT

We thank Markus Drechsler for cryo-TEM measurements and André Gröschel for help with some graphics. This research is supported by the DFG within SFB 840 (TP A1). A. Wolf acknowledges support by BayEFG.

REFERENCES

(1) Perro, A.; Reculusa, S.; Ravaine, S.; Bourgeat-Lami, E. B.; Duguet, E. *J. Mater. Chem.* **2005**, *15*, 3745–3760.
(2) Walther, A.; Müller, A. H. E. *Soft Matter* **2008**, *4*, 663–668.
(3) Walther, A.; Drechsler, M.; Müller, A. H. E. *Soft Matter* **2009**, *5*, 385–390.
(4) Wurm, F.; Kilbinger, A. F. M. *Angew. Chem., Int. Ed.* **2009**, *48*, 8412–8421.
(5) Walther, A.; Drechsler, M.; Rosenfeldt, S.; Harnau, L.; Ballauff, M.; Abetz, V.; Müller, A. H. E. *J. Am. Chem. Soc.* **2009**, *131*, 4720–4728.
(6) Yuet, K. P.; Hwang, D. K.; Haghgooie, R.; Doyle, P. S. *Langmuir* **2009**, *26*, 4281–4287.
(7) Jiang, S.; Chen, Q.; Tripathy, M.; Luijten, E.; Schweizer, K. S.; Granick, S. *Adv. Mater.* **2010**, *22*, 1060–1071.
(8) Glaser, N.; Adams, D. J.; Böker, A.; Krausch, G. *Langmuir* **2006**, *22*, 5227–5229.
(9) Ruhland, T. M.; Gröschel, A. H.; Walther, A.; Müller, A. H. E. *Langmuir* **2011**, *27*, 9807–9814.
(10) Walther, A.; Matussek, K.; Müller, A. H. E. *ACS Nano* **2008**, *2*, 1167–1178.
(11) Ling, X. Y.; Phang, I. Y.; Acikgoz, C.; Yilmaz, M. D.; Hempenius, M. A.; Vancso, G. J.; Huskens, J. *Angew. Chem., Int. Ed.* **2009**, *48*, 7677–7682.
(12) Kaufmann, T.; Gokmen, M. T.; Wendeln, C.; Schneiders, M.; Rinnen, S.; Arlinghaus, H. F.; Bon, S. A. F.; Du Prez, F. E.; Ravoo, B. J. *Adv. Mater.* **2011**, *23*, 79–83.
(13) Walther, A.; Göldel, A.; Müller, A. H. E. *Polymer* **2008**, *49*, 3217–3227.
(14) Zhang, K.; Gao, L.; Chen, Y. *Polymer* **2010**, *51*, 2809–2817.
(15) Erhardt, R.; Böker, A.; Zettl, H.; Kaya, H.; Pyckhout-Hintzen, W.; Krausch, G.; Abetz, V.; Müller, A. H. E. *Macromolecules* **2001**, *34*, 1069–1075.
(16) Liu; Abetz, V.; Müller, A. H. E. *Macromolecules* **2003**, *36*, 7894–7898.
(17) Walther, A.; André, X.; Drechsler, M.; Abetz, V.; Müller, A. H. E. *J. Am. Chem. Soc.* **2007**, *129*, 6187–6198.
(18) Conlon, D. A.; Crivello, J. V.; Lee, J. L.; Obrien, M. J. *Macromolecules* **1989**, *22*, 509–516.
(19) Li, M. Q.; Douki, K.; Goto, K.; Li, X. F.; Coenjarts, C.; Smilgies, D. M.; Ober, C. K. *Chem. Mater.* **2004**, *16*, 3800–3808.
(20) Kuo, S. W.; Tung, P. H.; Chang, F. C. *Macromolecules* **2006**, *39*, 9388–9395.
(21) Chen, S.-C.; Kuo, S.-W.; Liao, C.-S.; Chang, F.-C. *Macromolecules* **2008**, *41*, 8865–8876.

(22) Lee, N. S.; Sun, G.; Neumann, W. L.; Freskos, J. N.; Shieh, J. J.; Dorshow, R. B.; Wooley, K. L. *Adv. Mater.* **2009**, *21*, 1344–1348.
(23) Ober, C. K.; Li, M.; Douki, K.; Goto, K.; Li, X. *Photopolym. Sci. Technol.* **2003**, *16*, 347–350.
(24) Mountrichas, G.; Mantzaridis, C.; Pispas, S. *Macromol. Rapid Commun.* **2006**, *27*, 289–294.
(25) Yoshida, E.; Kuwayama, S. *Colloid Polym. Sci.* **2007**, *285*, 1287–1291.
(26) Hameed, N.; Liu, J.; Guo, Q. *Macromolecules* **2008**, *41*, 7596–7605.
(27) Ruiz de Luzuriaga, A.; García, I.; Mecerreyes, D.; Etxeberria, A.; Pomposo, J. A. *Polymer* **2010**, *51*, 1355–1362.
(28) Stepanek, M.; Matejicek, P.; Prochazka, K.; Filippov, S. K.; Angelov, B.; Slouf, M.; Mountrichas, G.; Pispas, S. *Langmuir* **2011**, *27*, 5275–5281.
(29) Auschra, C.; Stadler, R. *Polym. Bull.* **1993**, *30*, 257–264.
(30) Fernyhough, C.; Ryan, A. J.; Battaglia, G. *Soft Matter* **2009**, *5*, 1674–1682.
(31) Rolls, W.; Svec, F.; Fréchet, J. M. J. *Polymer* **1990**, *31*, 165–174.
(32) Jung, M. E.; Lyster, M. A. *J. Am. Chem. Soc.* **1977**, *99*, 968–969.
(33) Jung, M. E.; Lyster, M. A. *J. Org. Chem.* **1977**, *42*, 3761–3764.
(34) Plamper, F. A.; Becker, H.; Lanzendörfer, M.; Patel, M.; Wittemann, A.; Ballauff, M.; Müller, A. H. E. *Macromol. Chem. Phys.* **2005**, *206*, 1813–1825.